AIAA JOURNAL
Vol. 42, No. 2, February 2004

Investigation of the Symmetric Wetting of Vane–Wall Gaps in Propellant Tanks

Yongkang Chen* and Steven H. Collicott†
Purdue University, West Lafayette, Indiana 47907-2023

Symmetric wetting of a liquid in a vane–wall intersection with a gap is investigated. The geometry is common in surface tension propellant management devices (PMDs) in spacecraft liquid propellant tanks. A theoretical method is applied to determine a critical contact angle in the geometry for a range of parameters. The critical contact angle marks a division between the existence and nonexistence of a single-valued finite height equilibrium capillary surface spanning the entire cross section. When the contact angle is below the critical value, the capillary surface wicks up the gap, which is necessary for proper function of the PMD. The problem and results can also be viewed as determination of a critical gap size for a given contact angle. In addition to analysis, Surface Evolver simulations and drop tower experiments provide results in agreement with the analytical results. Drop tower results also demonstrate that the evolution of the wicking rate mimics that for a solid corner.

Nomenclature

A, A'	=	intersections of arc Γ with vane and tank wall surfaces
C	=	reentrant corner
L	=	nondimensional meniscus tip location
L'	=	dimensional meniscus tip location
M	=	intersection of line AA' with x axis
o	=	center of circular cross section of cylindrical container
R_γ	=	radius of arc Γ
S, u	=	single-valued equilibrium capillary surfaces
t	=	time
x	=	transverse coordinate
y	=	transverse coordinate
z	=	axial coordinate
α	=	half-corner angle
Γ	=	name or length of an arc
Γ_{cr}	=	critical arc
γ	=	contact angle
γ_{cr}	=	critical contact angle
δ	=	nondimensional gap size
$\tilde{\delta}$	=	dimensional gap size
ϵ	=	nondimensional vane thickness
$\tilde{\epsilon}$	=	dimensional vane thickness
ζ	=	absolute value of x coordinate of point A
θ	=	one-half of the angle that arc Γ spans
λ	=	absolute vlaue of x coordinate of point M
Σ	=	name and perimeter of cylindrical container cross section
Σ^*	=	length of subarc of Σ
σ	=	surface tension
Φ	=	functional
ϕ	=	one-half of the angle that Σ^* spans
Ω	=	name and area of cylindrical container cross section
Ω^*	=	area of subdomain of Ω

Presented as Paper 2002-3986 at the AIAA/ASME/SAE/ASEE 38th Joint Propulsion Conference, Indianapolis, IN, 7–10 July 2002; received 25 February 2003; revision received 3 October 2003; accepted for publication 6 October 2003.

*Research Assistant, School of Aeronautics and Astronautics. Member AIAA.

†Associate Professor, School of Aeronautics and Astronautics. Associate Fellow AIAA.

Introduction

CAPILLARY flow in a vane–wall geometry (Fig. 1) is common in a vane-type propellant management device (PMD) in weightless operation in space. A vane-type PMD is widely used to position, control, and transport the liquid propellants in liquid propellant tanks. According to Jaekle,[1] among vane-type PMDs, a simple vane is used frequently because it is easy to build and provides adequate performance to meet the mass flow demands of the spacecraft. A simple vane is defined as a thin solid sheet that nominally meets the solid tank wall. A gap between the vane and the tank wall is generally present for several possible reasons. A modern ultralight satellite propellant tank is a thin-walled metallic liner and a composite overwrap for strength, and so welding the vane to the tank wall is not done. The gap may also be present to avoid problems, for example, of tank diameter changes with pressure or generating particulate debris from scratching of the vane on the tank wall. The existence of the gap creates concern about the re-wetting of the liquid propellant after maneuvers of the spacecraft. The acceleration generated by the firing pulls the propellant away from the zero-g equilibrium position. Afterward, the rewetting, if it exists, can transport the propellant back to the zero-g equilibrium position. Otherwise, if the gap between the vane and the tank wall is too large, rewetting will not occur, and the propellant will remain in the undesired location. Determination of how small of a gap is sufficiently small to create this important rewetting flow is the goal of this work. Because the successful design of the PMD is critical to the mission, variations in fluid control capabilities caused by the vane–wall gap need to be well understood.

In this paper, symmetrical configurations in which a vane is perpendicular to a cylindrical tank wall are studied. Furthermore, to be general and simple, the analysis is restricted to the geometrical configuration in which both the vane and the container have infinite height. The numerical modeling can be construed to be either finite or infinite in extent, and the drop-tower experiment is, of course, finite in height. Analysis for the infinite height tank can now be extended to other geometries by use of the Surface Evolver code, as validated for the Concus–Finn critical contact angle analysis by Collicott and Weislogel[2] (see Refs. 3–7).

A theoretical method was initially developed by Concus and Finn[3] and furthered by Finn,[4,5] Finn and Leise,[6] and Finn and Neel[7] to provide an existence criteria for single-valued finite height equilibrium capillary surfaces in a cylindrical container of general cross section (Fig. 2). In the context of their theory, a single-valued finite height equilibrium capillary surface is a smooth, bounded interface (surface) of the liquid that completely covers the base of the container. According to Concus–Finn theory, for liquid in a cylindrical container of arbitrary cross section in zero-gravity, only the shape of

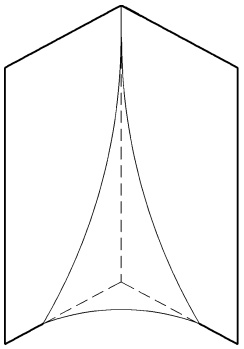

Fig. 1a Capillary menisci in a solid interior corner.

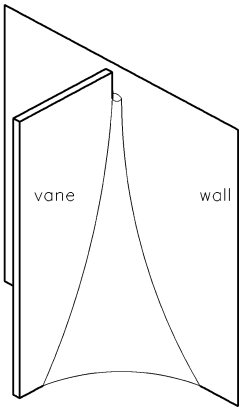

Fig. 1b Vane–wall junction with a gap.

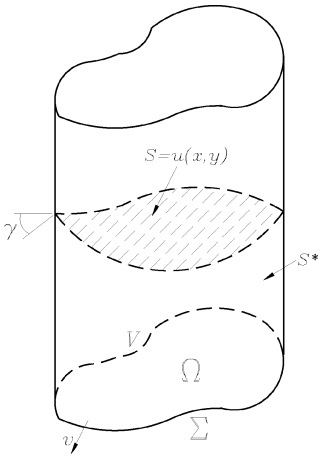

Fig. 2 Generic cylindrical tank, γ is the contact angle between the normal vectors for the wall and the interface at the contact line (common definition of contact angle measured in the liquid phase).

the cross section and the contact angle of the liquid γ determine the existence of the single-valued finite height equilibrium capillary surface. General geometries of the cross section, referred to as type 1 and type 2, are shown in Fig. 3. A reentrant corner, such as one end of a thin vane, is present in the type 2 geometry.

A major part of the application of the Concus–Finn theory is to determine critical circular arcs Γ_{cr} of radius $R_\gamma = \Omega/(\Sigma \cos\gamma)$ in the cross section that meet the walls at an angle γ (and similarly, as explained hereafter, for meeting a corner) and make a functional Φ vanish. The functional Φ is introduced hereafter, but details must be sought in the numerous references by Concus and Finn. That is, this paper serves to report an application of the theory and does not seek to repeat the development of the theory. When $\Phi = 0$, the corresponding contact angle is called the critical contact angle γ_{cr}. When the contact angle γ (measured in the liquid phase) is greater than γ_{cr}, then the finite height single-valued equilibrium capillary surface $S = u(x, y)$ exists, and so rewetting does not occur. When $\gamma < \gamma_{cr}$, the finite height single-valued equilibrium capillary surface

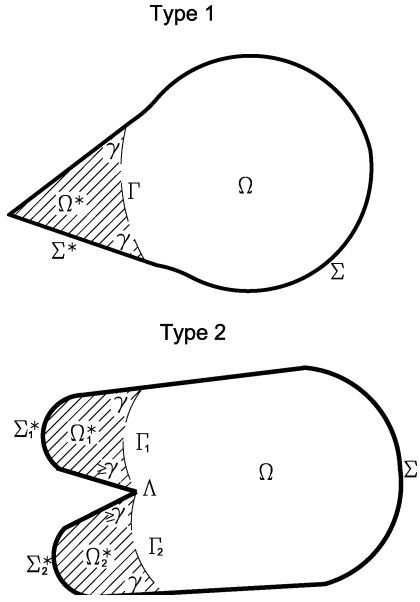

Fig. 3 General domain Ω and $\{\Gamma; \gamma\}$ configuration.

$S = u(x, y)$ fails to exist, and a rewetting flow in the region of higher curvature ensues. The existence of such a surface at precisely $\gamma = \gamma_{cr}$ differs for different cross sections[8] and is determined for the vane–wall gap geometry.

This method was applied by Concus and Finn to study numerous geometries such as a wedge as described hereafter, a trapezoid, a bathtub, a keyhole, etc.[9,10] It was also applied by Smedley[11] to study an eccentric annular cross section. Experimental studies performed by Langbein et al.[12] and Smedley[13] have confirmed some of these analytical results. The geometry in this study was addressed inconclusively with Surface Evolver by Collicott and Weislogel.[14]

The key feature of the vane–wall with gap geometry in this study is two corners formed between the vane and the tank wall connected by a gap in between them. The existence of the gap is an important addition that makes the two corners not simply two interior corners any more (Fig. 1). The existence of the equilibrium capillary surface in an interior corner under zero-gravity was studied by Concus and Finn.[3,15–17] They found that the critical contact angle for an interior corner is

$$\gamma_{cr} = \pi/2 - \alpha \tag{1}$$

where α is one-half of the corner angle. For a cylindrical container of regular polygonal cross section, when $\gamma_{cr} \le \gamma \le 90$ deg, liquid of sufficient volume would cover the base and yield a single-valued interface of finite height. (Smaller volumes of liquid would result in dry spots on the end of the cylinder, but the same physics in the corner.) Otherwise, when $\gamma_{cr} > \gamma$, the liquid would move up along the corners because of an unbalanced pressure gradient toward the meniscus tip, until it reaches the top of the container or until part the base starts to dry out, limiting the amount of liquid available for wicking up the corner. In a liquid propellant tank, $\gamma_{cr} > \gamma$ implies the rewetting of the liquid, or the redistribution of the propellant to secure the provision of the propellant after maneuvers, which is essential to the performance of the PMD. For the vane–wall gap corner, the presence of the gap changes the structure of the interface surface near the tip of the meniscus. Thus, any effects that this change would bring about on the Concus–Finn critical contact angle γ_{cr} need to be understood.

The analytical method is briefly outlined and is followed by its application to the geometry under investigation. This paper then presents Surface Evolver simulations to determine the equilibrium capillary surface profile and to identify the critical contact angle numerically. In the last part of the paper, some results obtained from drop-tower experiments are reported.

Methods

Analytical Method

The analytical method developed by Concus and Finn is outlined briefly hereafter. This overview does not rederive or fully explain the theory but is meant to provide the link, through discussion and figures, for readers to understand the application of the established theory to a new geometry. Details can be found in Refs. 4–7.

Consider a cross section of the cylinder, shown in Fig. 2, that is normal to the axis of the container, as shown in Fig. 3. In Fig. 3, the domain Ω in a type 1 geometry is bounded by the arc Γ that meets the wall at angle γ, whereas in a type 2 geometry Γ can terminate at the corner, subject to a different angle constraint.[5] The point C exists on the boundary of Ω and forms an angle greater than 180 deg measured from inside of Ω. Thus, C is called a reentrant corner.

Based on the theory by Concus and Finn, assume that the free surface intersects the cross section along an arbitrary circular arc Γ of radius R_γ that is given by

$$R_\gamma = \Omega/\Sigma\cos\gamma \tag{2}$$

meets the boundary wall at γ and meets the reentrant corner point at an angle $\geq\gamma$. The arc Γ, together with a subarc $\Sigma^* \subset \Sigma$, bounds a subdomain $\Omega^* \subset \Omega$. A functional is defined as

$$\Phi(\Gamma) = \Gamma - (\cos\gamma)\Sigma^* + (\Sigma\cos\gamma/\Omega)\Omega^* \tag{3}$$

over the subdomain Ω^*. Concus and Finn theory shows that a single-valued finite height equilibrium capillary surface exists for given Ω and γ if and only if the functional Φ is positive. When Φ=0, such an interface may or may not exist, depending on the geometry.

More specifically, for every such an arc Γ, if $\Phi > 0$, then the liquid free surface extends to a finite height inside the cylinder throughout the cross section. If, for certain contact angles, there is an arc Γ that makes $\Phi \leq 0$, then no equilibrium capillary surface will be found for that contact angle. In other words, the free surface extends to infinite height in the subdomain Ω^*. The contact angle for which $\Phi = 0$ is called the critical contact angle, or Concus–Finn angle, and is denoted here as γ_{cr}. The corresponding arc Γ is called the critical arc, denoted as Γ_{cr}. Normally, there are at most a finite number of arcs Γ that can be drawn; therefore, it is possible to evaluate Φ for a finite number of cases.

For every contact angle $\gamma < \gamma_{cr}$, where Φ is nonpositive, there possibly exists one singular solution, called a C-singular solution.[7] For this solution, within the domain $\Omega\backslash\Omega^*$, a solution $u(x, y)$ is determined up to an additive constant, or, in other words, the capillary surface S meets $\Sigma\backslash\Sigma^*$ at γ and it approaches an arc Γ_0 of radius $R_0 \geq R_\gamma$ asymptotically and extends up to infinite height; thus, $u \to \infty$ on Γ_0. This, too, implies rewetting of the gap as needed for PMD operation.

In this study, the cross section geometry is formed when a rectangle is surrounded with a circle. The liquid is contained in the region between the rectangle and the circle. Although the topology of this geometry is different from that of a generic cylindrical container, R. Finn pointed out (private communications, 2002) that the theoretical method described earlier can still be applied, as in non-concentric cylinders studied by Smedley.[11] A detailed description of the procedure of searching for the critical arc Γ_{cr} in this geometry is provided hereafter.

Application of the Theory

Application of the Φ functional method requires that each term of Eq. (3) be defined. For this purpose, the cross section geometry is shown in Fig. 4. Denote the thickness of the vane as ϵ and the gap size as δ. The inner radius of the cylinder is unity, and, because of this, ϵ and δ can be treated as nondimensional. In this study, one end of the vane is fixed at the center of the circle, point o, and the gap size is varied by changing the radial extent (width, hereafter) of the vane. Because of the symmetry of the configuration, all of the relevant quantities can be found in the upper half of the domain and

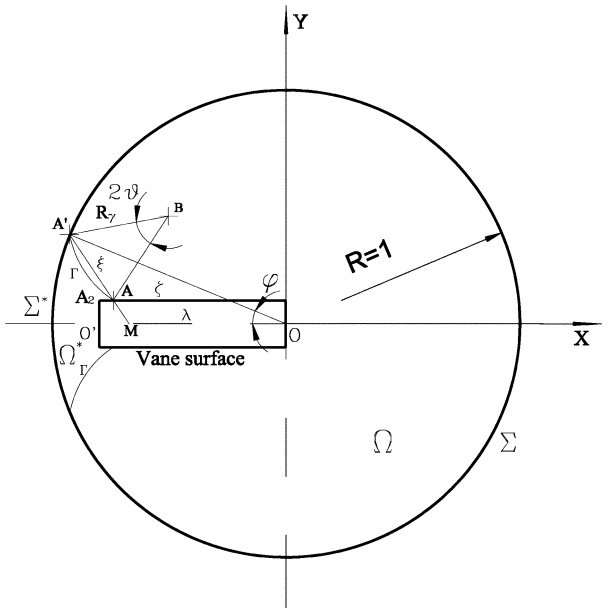

Fig. 4 Problem domain for the vane–wall gap geometry and $\{\Gamma;\gamma\}$ configuration.

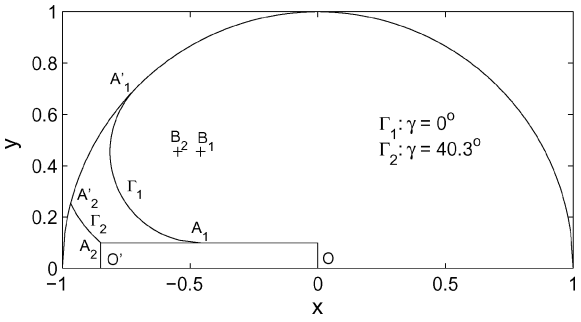

Fig. 5 Limiting critical arcs Γ of type 1 for $\epsilon = 0.2$ and $\delta = 0.15$.

then doubled to obtain the entire amount. Consequently,

$$\Omega = \pi - (1-\delta)\epsilon \tag{4}$$

$$\Omega^* = \varphi - \lambda\sin\varphi - (\epsilon/2)[2(2-\delta) - \zeta - \lambda] - \left(2R_\gamma^2\vartheta - \xi R_\gamma\cos\vartheta\right) \tag{5}$$

$$\Sigma = 2\pi + 2(1-\delta) + 2\epsilon \tag{6}$$

$$\Sigma^* = 2[\varphi + \epsilon/2 + (1-\delta-\zeta)] \tag{7}$$

where

$$\lambda = -x_M, \qquad \zeta = -x_A$$

$$\xi = AA' = \sqrt{(x_A - x_{A'})^2 + (y_A - y_{A'})^2}$$

$$\varphi = \arctan(y_{A'}/x_{A'}), \qquad \vartheta = \arcsin(\xi/2R_\gamma)$$

Points A and A' are intersections of the arc Γ with the vane surface and the cylindrical wall, respectively. Point M is the intersection of line $A'A$ with the x axis.

Once the geometric parameters ϵ and δ are set, then for every contact angle γ, one can obtain R_γ, the radius of the arc Γ, and then the points A and A' are found numerically by some standard method.

Consider, for example, a case where $\epsilon = 0.2$ and $\delta = 0.15$. It is found that there are two possibilities for the arc Γ:

1) The arc Γ meets both the cylindrical wall and the vane surface at angle γ, as shown in Fig. 5. Such arcs at two extreme locations are shown in Fig. 5, in which B_1 and B_2 denote the centers of the

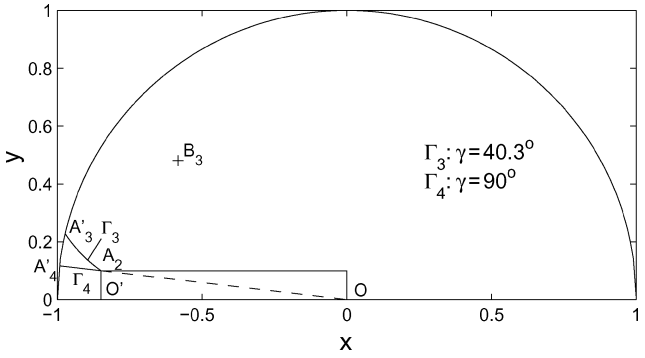

Fig. 6 Limiting critical arc Γ of type 2 for $\epsilon = 0.2$ and $\delta = 0.15$.

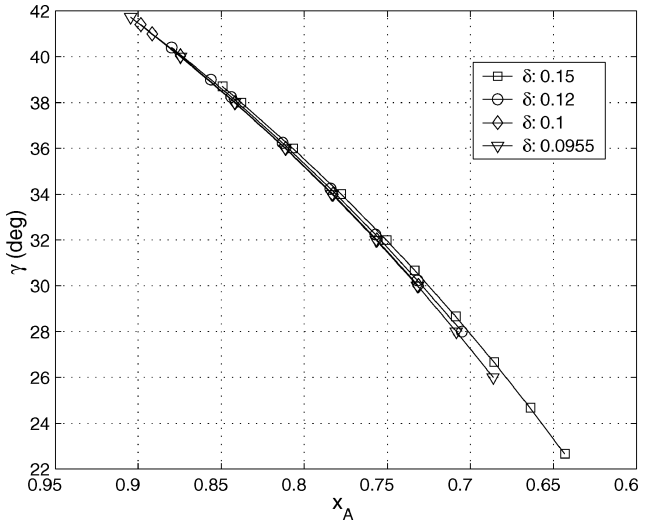

Fig. 7 Locations of the contact point of arc Γ with the vane surface for different gap sizes and contact angles with vane thickness $\epsilon = 0.1$.

arcs. Arc Γ_1 is for $\gamma = 0$ deg, and arc Γ_2 is for $\gamma = 40.3$ deg. Note that along with the increase of the contact angle from 0 to 40.3 deg, the contact points move from A_1 and A_1' to the points A_2 and A_2', respectively. Arcs of this type fail to exist for this δ and ϵ when $\gamma > 40.3$ deg.

2) The arc Γ starts at the corner vertex A_2 of the vane on one end and meets the cylindrical wall at angle γ on the other end, as shown in Fig. 6. Corner A_2 is a reentrant corner, and it is a requirement that the angle at which Γ meets the side A_2O' should be not less than γ, whereas the angle at which Γ meets the other side of the corner A_2 should be not less than $\pi - \gamma$. For 90 deg, the radius of the arc is infinite, so that the arc Γ will simply be a straight line connecting the point A_2, A_4' that is obtained by intersecting the line OA_2 with the circle.

In this example, when $\gamma \leq 40.3$ deg, one can have an arc of type 1 that satisfies the requirements of the theory. However, when $\gamma > 40.3$ deg, there is an arc Γ of type 2. Note that the large contact angle limit of the type 1 arcs Γ_2 is itself a type 2 arc, shown as Γ_3 in Fig. 6.

This process can be better understood with Figs. 7 and 8. Locations of point A on the vane surface for different contact angle and gap size for a fixed vane thickness are shown in Fig. 7. For all gap sizes, point A is closer to the left (gap) end of the vane for large contact angle. Corresponding values of functional Φ for these contact angles can be found in Fig. 8. Note that the location where Φ changes sign is closer to the left (gap) end of the vane for smaller gaps. For the vane thickness of 0.1, as shown, and a gap smaller than 0.0955, one has to seek critical arcs of type 2.

In the general case, the functional Φ is computed for either type 1 or 2 arcs and the corresponding critical contact angles are obtained for a series of vane thickness and the gap size. These values, $\gamma_{cr} = \gamma_{cr}(\epsilon, \delta)$, are plotted against δ for each ϵ in Fig. 9. Note the dashed line in the middle of Fig. 9. In the region above the dashed line, the critical contact angle depends exclusively on an arc Γ of type 2. In the region below the dashed line, critical contact angles are found for the arc Γ of type 1. The vane–wall with gap geometry is a combination of corners and a gap. In the region above the dashed line, the determination of the critical contact angle is dominated by the gap; in the region below the dashed line, it is dominated by the corner.

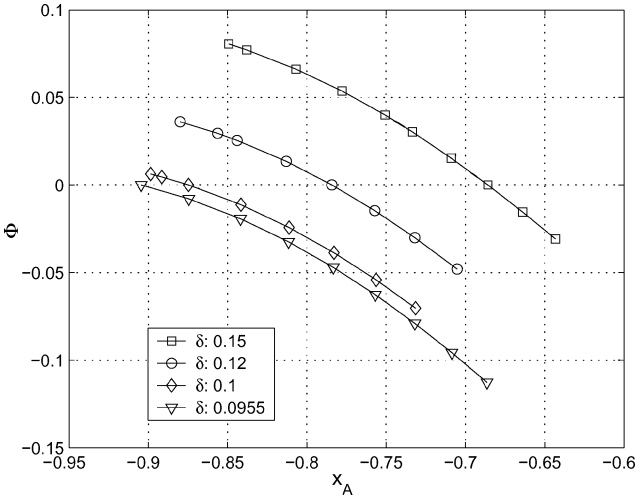

Fig. 8 Functional Φ values for different gap sizes and contact angles with vane thickness $\epsilon = 0.1$.

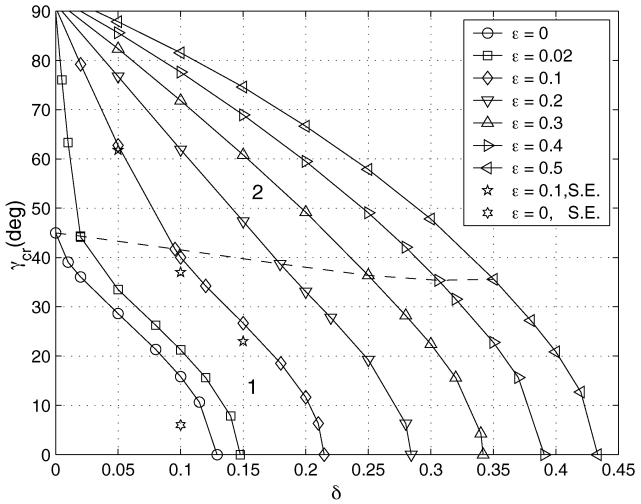

Fig. 9 Critical contact angle γ_{cr} vs gap size δ: ——, analysis and ☆, Surface Evolver simulation; approximately horizontal dashed line divides the regions where the critical contact angle is determined by the arc Γ of types 1 and 2 as labeled.

In Fig. 9, each curve defines γ_{cr} as a function of δ. Alternately, the results can be viewed as defining a critical δ, denoted as δ_{cr}, for every γ. Again, each curve divides the first quadrant into two parts. In the part above the line, there is always a single-valued finite height equilibrium capillary surface in the cylinder. In the region on or below the line, there can be no single-valued finite height equilibrium capillary surface. Analogously, the results can be viewed as defining a region to the right of the curve where the gap is too large to cause the rewetting of the corners, whereas on or left of the line, the gap is sufficiently small to permit the liquid to rewet the corners as desired for PMD operation.

Near the upper left corner of the plot, all of the curves of nonzero ϵ approach $\gamma_{cr} = 90$ deg. These curves approach, but do not terminate, at 90 deg because, when the vane touches the cylindrical wall surface, the gap disappears and two separate solid interior corners are

formed. Each of these two interior corners will have $\gamma_{cr} = \pi/2 - \alpha$ as determined by the Concus–Finn condition, where α is one-half of the corner angle. Thus, there is a discontinuity in γ_{cr} as $\delta \to 0$, showing that there is a substantial difference between even a very small gap and a true corner. Note, too, that for a finite thickness vane ($\epsilon > 0$) with $\delta \ll \epsilon$, the gap geometry resembles the parallel-plate wicking geometry studied by Dreyer et al.,[18] who found that, for the contact angle close to zero, the wicking of liquid in the gap between the plates ceases when the ratio of gap size over the width of the plate is greater than or equal to 1. The plates widths in Ref. 18 ranged 17.8 to 50.8 mm.

Surface Evolver Modeling

In this study, Surface Evolver[19] is applied to determine numerically the critical contact angle for several specific geometric parameters. Use of Surface Evolver in addition to the preceding analysis is not a simple redundancy because when $\gamma > \gamma_{cr}$, Surface Evolver provides the three-dimensional surface shape throughout the cross section. Also, through comparison of the analytical and Surface Evolver results, the validity of the Surface Evolver model in this type of problem is confirmed, thereby permitting future solutions in geometries not amenable to the infinite cylinder approach of the Concus–Finn analysis (for example, sphere tanks with vanes, tapered vanes, inconsistent gap sizes, etc.).

Surface Evolver minimizes the energy of a surface subject to various user-defined constraints by the use of a gradient descent or other minimization methods. A constraint can be a quantity integrated over a surface, or it can be a quantity constant such as a volume. A constraint can also be a geometric constraint such as a wall through which the surface is not to penetrate. For the zero-gravity interface in this study, the energies include the free surface energy and the interfacial energy between the liquid and the solid wall. With cylinder radius of unity as described earlier, ϵ and δ are nondimensional, and energies are nondimensionalized by the product of surface tension and radius (unity) squared. More fundamentally, without gravity or accelerations, the problem is a geometrical problem with results determined by shape, ϵ, and δ, and contact angle γ, not by the magnitudes of fluid properties. If a case of an accelerating spacecraft is to be considered, then a constant acceleration in any direction can be added to the Surface Evolver definition, as in Ref. 20, and then the magnitudes of density and surface tension enter the problem.

For practical wetting problems, Surface Evolver was originally applied by Tegart[21] (with input from Brakke) to study fluid interfaces in a circular cylindrical container, and by Brakke[22] followed by Collicott et al.,[23] Bayt and Collicott,[24] and Chen and Collicott[25] to investigate both statics and stability problems of a ullage bubble in the large toroidal spinning liquid helium tank of the Gravity Probe-B satellite. Surface Evolver has been validated against experiment in a 1-g version of the Gravity Probe-B problem,[23] classical instability theory and Concus–Finn theory in a solid corner,[2] and against predictions of Concus–Finn angle for rounded rectangles.[14] Grid convergence, resolution, and similar details of the use of Surface Evolver to compute Concus–Finn critical angles are given in Ref. 2.

Geometry and Constraints

For this study, the computational domain is the same as shown in Fig. 4, where $y = 0$ is the symmetry plane. To speed up the computation, one-half of the interface surface was simulated due to the symmetry of the geometry. This restricts the modeling to surfaces symmetric about the plane of the vane, as in the preceding application of the critical contact angle theory of Concus and Finn. There are cases where symmetric containers have asymmetric solutions of lower energy than symmetric solutions, and so, in general, such possibilities need to be considered. The space shuttle experiment axisymmetric containers of Concus et al.[26] is the most authoritative example. Recent Surface Evolver analysis of asymmetric propellant positioning in PMDs with two symmetry planes shows that the phenomena is relevant to spaceflight systems.[27] In the present geometry, the drop-tower experiments have yet to show any evidence of growth toward an asymmetric solution, in spite of the inevitable but small asymmetries of any manufactured device such as the test cell.

Table 1 Definition of quantities for Surface Evolver studies

Case	ϵ	δ	γ, deg
1	0.1	0.05	N/A
2	0.1	0.1	N/A
3	0.1	0.15	N/A
4	0	0.1	N/A
5	0.1	0.2	0
6	0.1	0.25	0

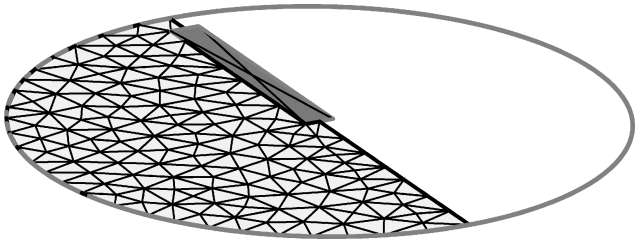

Fig. 10 Initial surface in the Surface Evolver simulation.

An example initial surface in the Surface Evolver simulation is shown with 259 triangular facets in Fig. 10. The geometric constraints defined in Surface Evolver for this task include the cylindrical wall and the finite thickness vane surface. It is assumed that the cylindrical container and vane are of infinite length and uniform cross section and that there is always sufficient liquid to cover the base of the container.

The vane thickness ϵ, gap size δ, and contact angle of the liquid on the tank wall and vane surface, γ, are variable. Whereas the gap must clearly be spanned by more than one facet, the minimum number of facets to span the gap and produce an accurate answer is not known and requires futher study. The small gap in a large tank ($\delta \ll 1$), combined with the need for Surface Evolver to run with a small range of facet areas leads to large numbers of facets in these simulations. That is, the small facets required to resolve the free surface curvature in the gap must also be used to model the bulk of the free surface where curvature is not strong. In the computation, the initial number of facets was approximately 4096, or (2^{12}); however, more facets are produced in the refinement steps of running Surface Evolver and also by the increase of the free surface area as liquid wicks up the gap. This automated grid management is an important part of computing these solutions.

Surface Evolver Results

Definitions of the quantities in four cases of Surface Evolver modeling are presented in Table 1. The critical contact angle results of the first four cases are plotted in Fig. 9. Additionally, the interface profiles on the $y = 0$ plane, where the capillary surface has both maximum and minimum points and the contact line on the vane surface is extracted from the Surface Evolver results. The contact lines from case 1 are shown in Fig. 11, where $z = 0$ is the initial location of the surface. The x-direction extent of the vane is marked by two vertical dotted lines. The solid curves between these dotted lines are the contact lines on the vane surface. The lines outside the vane region represent the interface profiles in the container symmetry plane, $y = 0$. The meniscus tip is located in the gap region between $-1 < x < -0.95$. The meniscus tip is higher for small contact angle. In the region between $x = 0$ and $x = 1$, the interface is lower for small contact angle. All of the lines are well-converged data, except for the $\gamma = 61.8$ deg curve for which $\gamma < \gamma_{cr}$. In theory, the interface will rise infinitely high, and in Surface Evolver, it will rise as high as compute time and other resources permit if regridding is automated.

The necessarily unconverged $\gamma = 61.8$ deg case is shown in Fig. 11 to illustrate how the contact line on the vane surface sticks to the edge of the vane at $x = -0.95$ (the vertical solid line obscuring

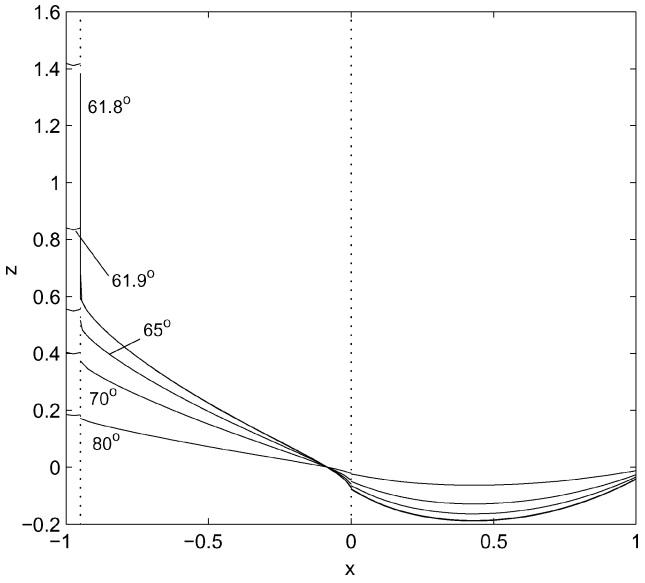

Fig. 11 Interface profiles on $y = 0$ and contact lines on the vane surface for different contact angles, as denoted, $\epsilon = 0.1$ and $\delta = 0.05$.

Fig. 12 Interface surface for $\epsilon = 0.1$, $\delta = 0.05$, and $\gamma = 65$ deg; well converged.

the dotted line). Recall from the preceding analysis that for $\epsilon = 0.1$ and $\delta = 0.05$, the $\gamma_{\rm cr}$ is determined by an arc Γ of type 2. This vertical portion of the interface on the edge of the vane must also lie on the arc Γ determined by the contact angle γ. (Therefore, the asymptotic approach of part of the surface with finite height to the arc Γ discussed earlier does exist in this case.) An equilibrium capillary surface under zero gravity is a surface of constant mean curvature. In this case, once the vertical portion of the surface sticking to the edge of the vane appears, the further increase of the length of this portion would not change the curvature difference between it and the surface in the gap area, nor in the domain Ω^*. In addition, at this stage, the surface on the domain $\Omega \backslash \Omega^*$ and on Γ has a constant mean curvature. Based on this, it can be concluded that the surface in the gap area would proceed to infinite height, and 61.8 deg can be identified as $\gamma_{\rm cr}$ for this case. However, the analytical value is 62.76 deg for an error in the Surface Evolver result of approximately 1.5%. As in many problems where a continuum is discretized, more computational power would reduce the uncertainty in Surface Evolver results for the Concus–Finn critical contact angle.[2]

Figures 12 and 13 present the (one-half) surfaces in a three-dimensional view of case 1 with $\gamma = 65$ and 61.8 deg. In Figs. 12 and 13, the edges of individual facets are not shown. The cylindrical tank surface is represented by the circle, and the vane rectangle in the middle of the circle that is partly hidden by the interface.

For case 2 ($\epsilon = 0.1$ and $\delta = 0.1$), as shown in Fig. 14, a similar pattern to the case 1 results is observed. Variations of the interface profile, contact line, and meniscus tip vs contact angle can be discerned. Only the data for $\gamma = 37.4$ deg are not a converged solution. For $\gamma = 37.4$ deg, the interface profile on $y = 0$ and contact lines on the vane and the cylinder wall are shown in Fig. 15. The vertical dashed lines at $x_A = -0.8323$ and $x_{A'} = -0.9736$ mark the

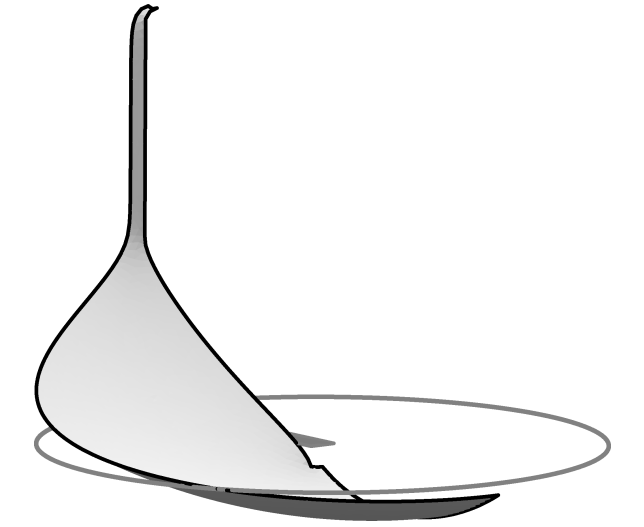

Fig. 13 Interface surface for $\epsilon = 0.1$, $\delta = 0.05$, and $\gamma = 61.8$ deg; not converged.

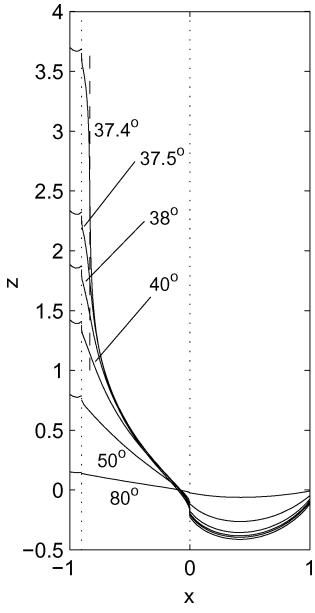

Fig. 14 Interface profile on $y = 0$ and the contact line on the vane surface for different contact angle values as denoted, $\epsilon = 0.1$ and $\delta = 0.1$.

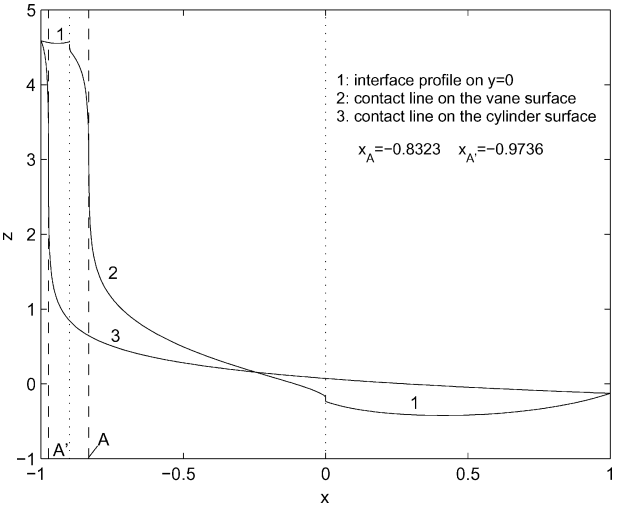

Fig. 15 Interface profile on $y = 0$, the contact line on the vane surface, the contact line on the cylindrical surface projected to x–z plane: $\epsilon = 0.1$, $\delta = 0.1$, and $\gamma = 37.4$ deg.

x coordinates where the arc Γ for $\gamma = 37.4$ deg meets the vane A and the cylinder wall A'. Asymptotic-like behavior of the contact lines near the dashed lines is evident. Figures 16 and 17 also present the surfaces in three-dimensional views of case 2 with $\gamma = 38$ deg and $\gamma = 37.4$ deg. According to the analysis, for this case, γ_{cr} is dependent only on the arc Γ of type 1. The asymptotic behavior of the contact line reveals the feature of the C-singular solution described in the analysis, and one can conclude that the meniscus tip would proceed to infinity. The Surface Evolver analysis produces

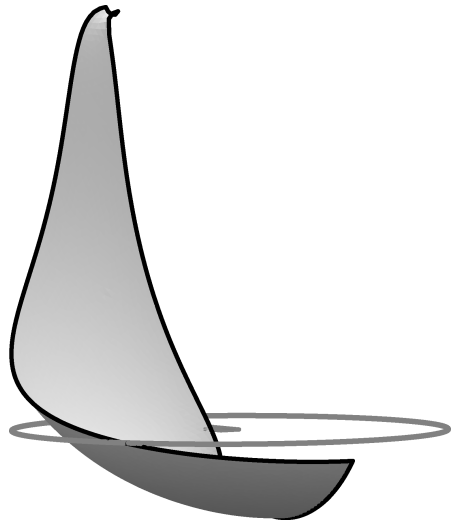

Fig. 16 Interface surface for $\epsilon = 0.1$, $\delta = 0.1$, and $\gamma = 38$ deg; well converged.

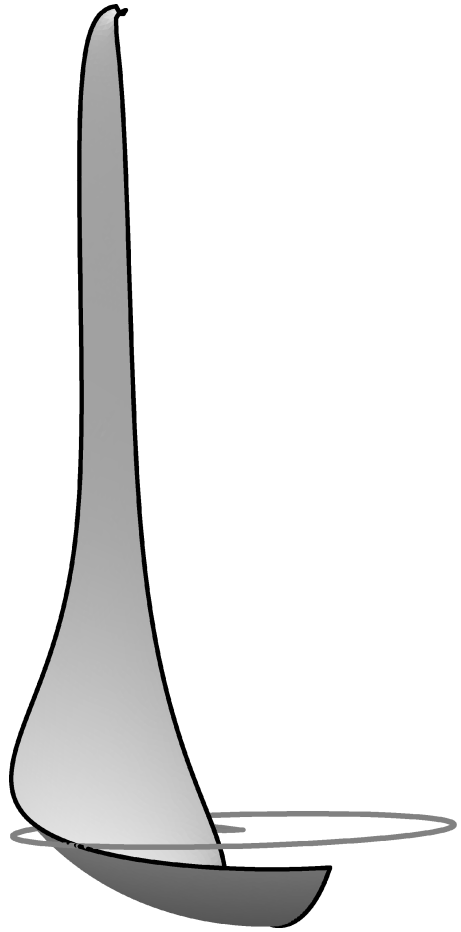

Fig. 17 Interface surface for $\epsilon = 0.1$, $\delta = 0.1$, and $\gamma = 37.4$ deg; not converged.

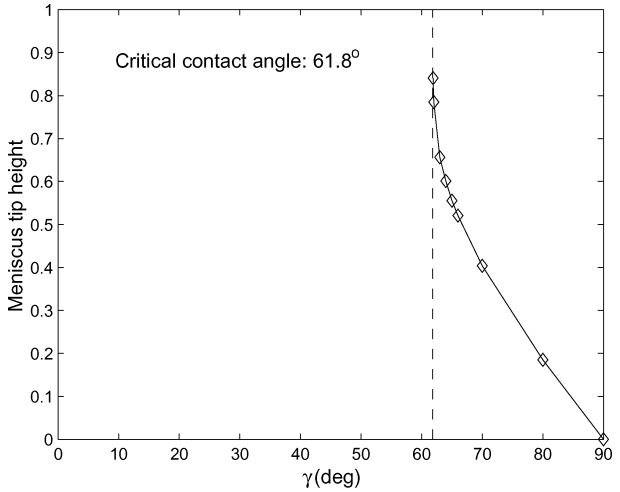

Fig. 18 Meniscus tip height vs contact angle for $\epsilon = 0.1$ and $\delta = 0.05$.

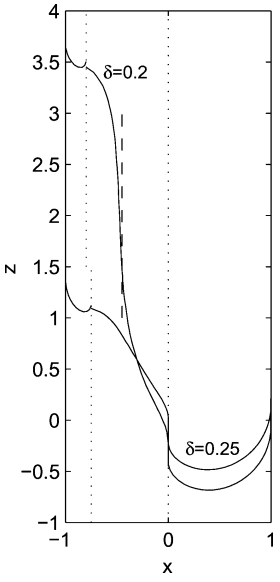

Fig. 19 Interface profile on $y = 0$ and the contact line on the vane surface, $\epsilon = 0.1$ and $\gamma = 0$ deg.

$\gamma_{cr} = 37.4$ deg, whereas the analytical value is 40.03 deg, less than a 7% difference.

In the same fashion, the critical contact angle obtained for case 3 ($\epsilon = 0.1$ and $\delta = 0.15$) is 23.3 deg, which is 13% off of the analytical value of 26.67 deg. For case 4 ($\epsilon = 0$ and $\delta = 0.1$), it is 6 deg with a 62% difference from the analytical value of 15.84 deg.

A method used by Concus et al.[28] to visualize γ_{cr} is also applied here. For case 1, the maximum meniscus height was collected and plotted against the contact angle. The results are shown in Fig. 18. It is evident that the meniscus height is relatively small until γ approaches γ_{cr} from above, and then the meniscus height increases rapidly with minute decreases in γ.

For cases 5 and 6, $\epsilon = 0.1$ and $\gamma = 0$ deg at two gap sizes, $\delta = 0.2$ and 0.25, respectively. According to the analysis, $\delta_{cr} = 0.215$ for $\epsilon = 0.1$ when $\gamma = 0$. The results are shown in Fig. 19. The surface of $\delta = 0.25$ is well converged, yet there is no hint of convergence for the $\delta = 0.2$ case. Again, the dashed line at $x = -0.4496$ is the location where the arc Γ meets the vane surface for $\delta = 0.2$, and one can see indications of asymptotic behavior of the contact line to the dashed line. These two results show that δ_{cr} falls between the two thickness values tested here.

Drop-Tower Experiment

The experimental study is conducted in the new design drop tower at Purdue University. This drop tower was constructed at the Aerospace Sciences Laboratory of the School of Aeronautics and Astronautics.[29] It became operational in the winter of 1999–2000. The tower is 28 ft high and provides about 1.27 s of microgravity

test time. The tower is constructed of acrylic tubes and is evacuated during the experiment. A system consisting of a stepper motor, an electromagnet, and a retrieval ring on fine string is set up inside the tower to drop cleanly and retrieve rapidly the test cell without breaking the vacuum. A digital imaging system, including a dropping charge-coupled device (CCD) camera, a stationary CCD camera on the ground, and a computer and software, is set up outside of the tower. This system enables acquisition of a large set of data in a single workday.

Two types of images are acquired. First, the dropping camera falls down along a track parallel to the tower, nominally equivalent to the dropping test cell. This camera transfers the images to the computer. Unfortunately, the drag force on the falling camera package and any contact with the alignment rail slows down the camera. Therefore, at some point, the test cell falls out of the field of view of the camera. The way to compensate this is to put another camera on the ground waiting for the test cell. The dropping camera captures images of the test cell from the beginning to somewhere around $0.8 \sim 0.9$ s. The camera on the ground captures an image before the test cell touches the cushion at about 1.27 s.

The test cell for the experimental work is shown in Fig. 20. The acrylic cylinder in the center part is a fluid cell with a piece of stainless-steel vane mounted near the cylinder wall. The cross section of the test cell is the same as that of the computational domain. The geometric parameters are listed in Table 2. The test cell is partially filled with silicon oil (polydimethylsiloxane), which has almost zero contact angle on both the acrylic and the stainless steel. The best vacuum inside the tower obtained with a mechanical pump is $300 \sim 400$ μmHg. Most of the data presented next were acquired at this vacuum level.

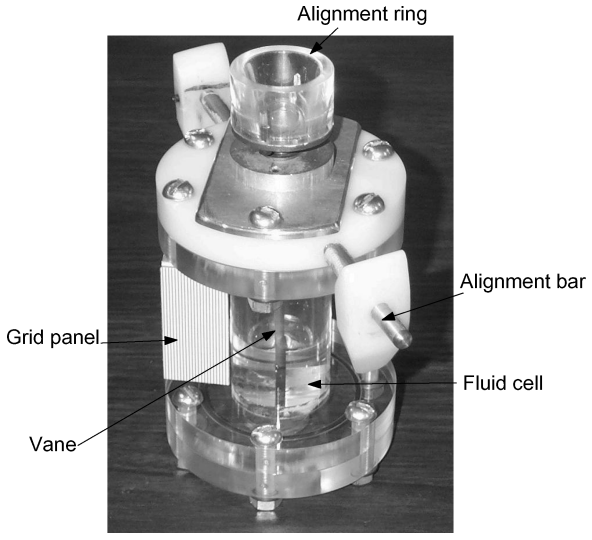

Fig. 20 Drop-tower test cell; transparent acrylic cylinder in the center is the fluid cell.

Experiment Results

The meniscus tip height is located and recorded as a function of time from the images of the test cell during free fall. MATLAB® was used to process the image data, and the meniscus tip was picked up manually by a cross hair. On most images, the tip can be identified obviously, so that no specific image processing is applied. However, the contrast of some of the images is poor, and it is reasonable to expect some error in determining the tip locations.

Results of the 0.05-in. (1.27-mm) thickness with gap size 0.025, 0.1, and 0.125 in. (0.635, 2.54, and 3.175 mm) are presented in Figs. 21–23. In these images, the width of the images is approximately the outer diameter of the fluid cell, which is 1.5 in. (38.1 mm). The tip of the meniscus can be identified very clearly. The contact line on the cylinder inner surface can also be identified on some images. These images reveal that the rising rate of the meniscus tip in the gap area decreases as the gap size increases. The tip locations at 1.267 s captured by the stationary camera are shown in Fig. 24. Up until this moment, it is evident in the images that the meniscus height is still increasing for $\tilde{\delta} = 0.025$, 0.05, and 0.1 in. (0.635, 1.27, and 2.54 mm). There is no obvious variation for $\tilde{\delta} = 0.125$ in. (3.175 mm).

Meniscus height vs time is shown in Fig. 25. The height is measured relative to the initial liquid surface level before the free fall. Figure 25 makes clear what one observes from the image data, that is, the tip height barely changes for $\tilde{\delta} = 0.125$ in. (3.175 mm).

Table 2 Parameters of the drop-tower experiment cross section geometry[a]

Gap size δ, in.	$\delta = \tilde{\delta}/r$
0.025	0.05
0.05	0.1
0.1	0.2
0.125	0.25

[a] All cases have cylinder radius of $\tilde{r} = 0.5$ in. and vane thickness $\tilde{\epsilon} = 0.1$, $r = 0.05$ in.

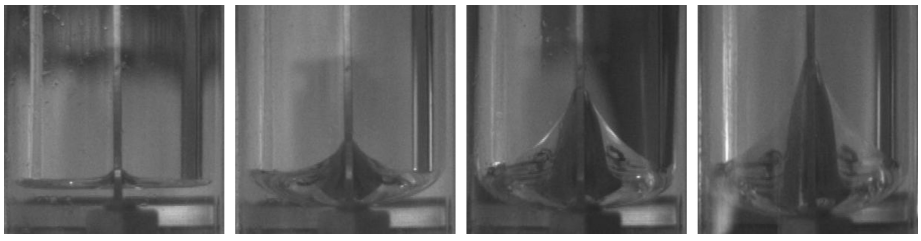

a) b) c) d)

Fig. 21 Meniscus at different times: a) 0, b) 0.1, c) 0.3, and d) 0.5 s; $\tilde{\delta} = 0.025$ in.

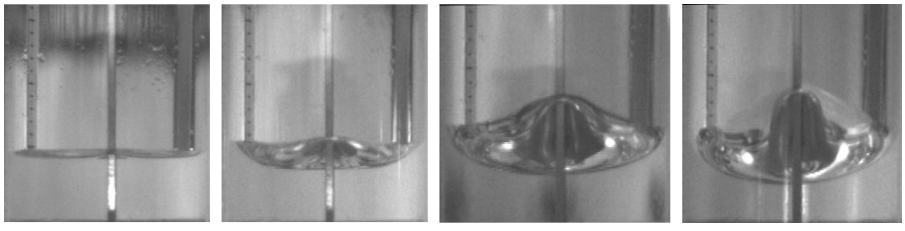

a) b) c) d)

Fig. 22 Meniscus at different times: a) 0, b) 0.1, c) 0.3, and d) 0.5 s; $\tilde{\delta} = 0.1$ in.

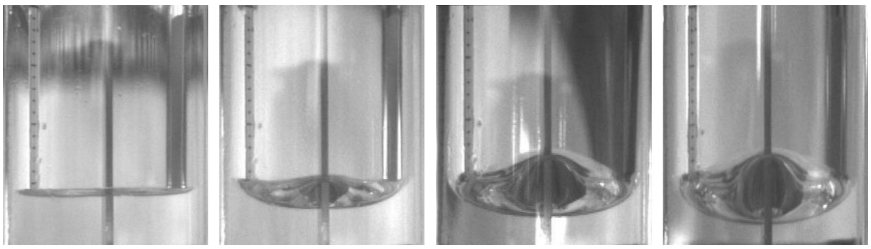

a) b) c) d)

Fig. 23 Meniscus at different times: a) 0, b) 0.1, c) 0.333, and d) 0.5 s; $\tilde{\delta} = 0.125$ in.

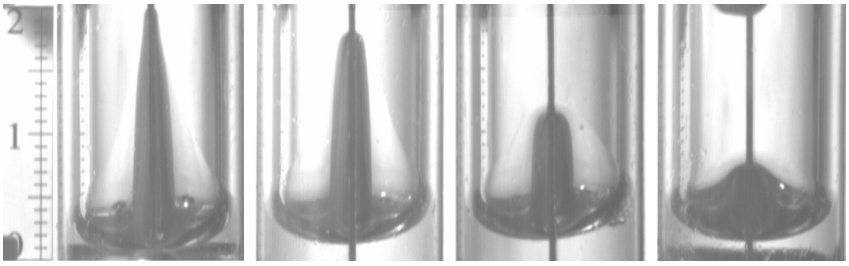

a) b) c) d)

Fig. 24 Meniscus at 1.267 s, $\tilde{\delta}$: a) 0.025, b) 0.05, c) 0.1, and d) 0.125 in.

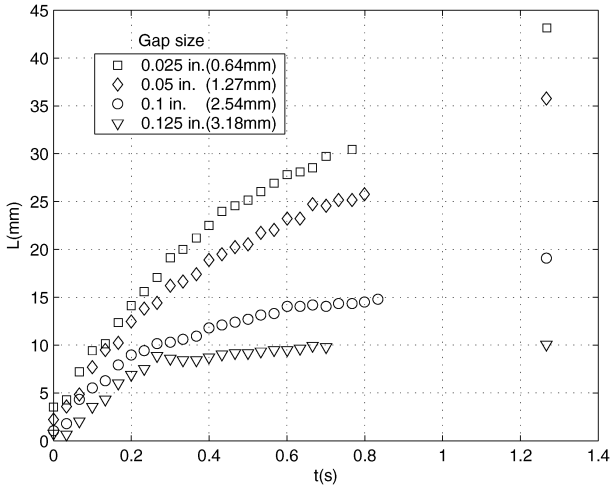

Fig. 25 Meniscus tip height as a function of time; vane thickness $\tilde{\epsilon}$ is 0.05 in.

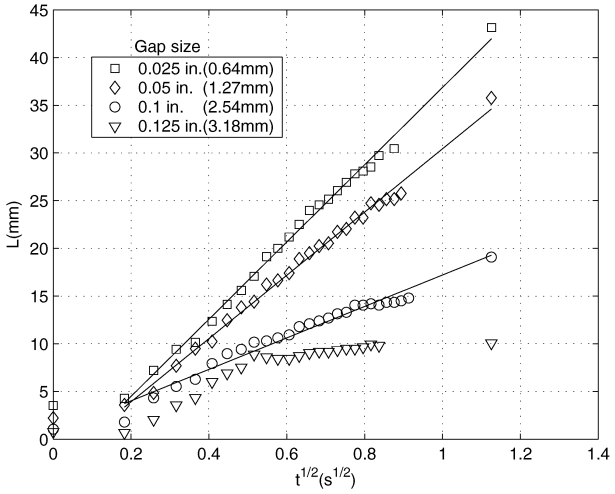

Fig. 26 Meniscus tip height in inches L as a function of $t^{1/2}(s^{1/2})$ with $L = c + mt^{1/2}$ line fits; vane thickness $\tilde{\epsilon}$ is 0.05 in. (Table 3 presents the coefficients of the linear fits.)

Table 3 Linear fit coefficients for capillary advance rate data of Fig. 26

$\tilde{\delta}$, in.	c, in.	m, in. $\cdot$ s$^{-1/2}$
0.025	−0.1425	1.594
0.05	−0.107	1.3052
0.1	−0.0284	0.6493

Using the radius of the circular cylinder to nondimensionalize the vane thickness and gap (Table 2), one can see that the nondimensional thickness is $\epsilon = 0.1$, and the gap size for 0.1 and 0.125 in. are $\delta = 0.2$ and 0.25, respectively. The drop time of 1.27 s is not as long as desired, but from the preceding discussion, one can still see that the critical gap size for $\epsilon = 0.1$ falls in the range between 0.2 and 0.25, which is favorable for analysis result $\delta_{cr} = 0.215$.

The data were rearranged and plotted against $t^{1/2}$, as shown in Fig. 26, because it is well known that the tip height $L \propto t^{1/2}$ in the range where the capillary flow is well developed in geometries such as the interior corner,[30] cylindrical capillary tube,[31] parallel plates,[32] and on a rod.[33] The coefficients of the fit are listed in Table 3. This treatment is approximate because the startup time for the capillary driven flow in this geometry was not estimated carefully. This might explain why the first several points for $\tilde{\delta} = 0.1$ in. drop out of the line.

For $\tilde{\delta} = 0.125$ in., the stabilized tip height is obtained as $\tilde{L} = 0.4$ in. (10.2 mm). Nondimensionalizing by cylinder radius gives a nondimensional tip height of 0.8. However, the Surface Evolver results show (Fig. 19) that the nondimensional tip height is around 1.37. This difference might be due to several causes: imperfection of the solid surfaces of the fluid cell and the vane, aerodynamic drag from the vacuum level inside the tower, and the accuracy of Surface Evolver simulation.

Conclusions

This study of symmetric liquid wetting behavior in a zero-gravity vane–wall gap is performed to support the design of surface tension PMDs that rely on thin vanes approaching the tank wall to form corners. Concus–Finn analysis, Surface Evolver modeling, and low-g experimentation combine to produce results that highlight the differences and similarities between this geometry and the simpler solid-corner geometry. The results show the following:

1) The existence of a single-valued finite height equilibrium capillary surface is characterized by the gap size, vane thickness, and

contact angle. When the vane thickness and the gap size are fixed, there exists a critical contact angle. On the other hand, when the vane thickness and the contact angle are fixed, there exists a critical gap size.

2) For each vane thickness and contact angle, there exists a threshold value of gap δ_{th}. For gap size $\delta < \delta_{\text{th}}$, the critical contact angle is dependent on the arc Γ of type 2, as described. For the gap size beyond δ_{th}, the critical contact angle is dependent only on the arc Γ of type 1.

3) For a given vane thickness and gap size, whenever the contact angle is below or equal to the critical contact angle, a single-valued finite height equilibrium capillary surface fails to exist. This also applies to the critical gap size for fixed vane thickness and contact angle. This lack of existence of a finite height single-valued interface indicates that the vane–wall junction can rewet after maneuverings, as desired in PMD design.

4) For the geometry in this study, a critical arc Γ_{cr} can be found, so that a single-valued finite height solution fails to exist for $\gamma = \gamma_{\text{cr}}$. However, for a container of regular polygonal cross section featured by interior corners, it is known that a single-valued finite height solution exists for $\gamma = \gamma_{\text{cr}}$. This difference results in continuous and discontinuous dependence of the interface on the boundary data, that is, the contact angle.

5) Surface Evolver proves to be a valid tool for prediction of the critical contact angle and determination of a solution surface in a singular sense. For the cases where a single-valued finite height equilibrium capillary surface fails to exist, a C-singular solution surface is identified for cases governed by an arc Γ of type 1. For the cases governed by a type 2 arc, a different singular solution was not found. However, the accuracy of the prediction of the critical contact angle needs to be improved via more extensive and careful refinement of the simulation.

6) Drop-tower testing produces agreement with critical gap size results of analysis and modeling, albeit at coarser resolution than analysis and modeling. The drop-tower tests indicate that when the gap size is less than its critical value, the wicking proceeds up the gap in a manner similar to the square-root of time results from the solid-corner wicking rate analysis of Weislogel.[30]

Acknowledgments

A gift from the Lockheed Martin Company, matched by the second author's National Science Foundation Career Award (CTS 95-01881), and a Purdue Research Foundation Fellowship for the first author enabled construction of the drop tower. The authors thank R. Finn of Stanford University, P. Concus of the University of California, Berkeley, and G. Smedley of Glaukos Corp. for their very helpful discussions of the analysis. Thanks also go to M. Weislogel of Portland State University for many suggestions and discussions on the experiments. K. A. Brakke's Surface Evolver user manual and code are both available at URL: http://www.susqu.edu/facstaff/b/brakke [cited 20 Aug. 2003].

References

[1]Jaekle, D. E., "Propellant Management Device Conceptual Design and Analysis: Vanes," AIAA Paper 91-2172, June 1991.

[2]Collicott, S. H., and Weislogel, M. M., "Computing Existence and Stability of Capillary Surfaces Using Surface Evolver," *AIAA Journal*, Vol. 42, No. 2, 2004, pp. 289–295.

[3]Concus, P., and Finn, R., "On Capillary Free Surfaces in the Absence of Gravity," *Acta Mathematica*, Vol. 132, 1974, pp. 177–198.

[4]Finn, R. A., "Subsidiary Variational Problem and Existence Criteria for Capillary Surfaces," *Journal fur die Reine und Angewandte Mathematik*, Vol. 353, 1984, pp. 196–214.

[5]Finn, R., *Equilibrium Capillary Surfaces, A Series of Comprehensive Studies in Mathematics*, Vol. 284, Springer-Verlag, New York, 1986, Chap. 6.

[6]Finn, R., and Leise, T. L., "On the Canonical Proboscis," *Journal for Analysis and Its Applications*, Vol. 13, No. 3, 1994, pp. 443–462.

[7]Finn, R., and Neel, R. W., "C-Singular Solutions of the Capillary Problem," *Journal fur die Reine und Angewandte Mathematik*, Vol. 512, 1999, pp. 1–25.

[8]Concus, P., and Finn, R., "Continuous and Discontinuous Disappearance of Capillary Surfaces," *Variational Methods for Free Surface Interfaces*, edited by P. Concus and R. Finn, Springer-Verlag, New York, 1987, pp. 197–204.

[9]Finn, R., "Existence Criteria for Capillary Free Surfaces Without Gravity," *Indiana University Mathematics Journal*, Vol. 32, 1983, pp. 439–460.

[10]Concus, P., and Finn, R., "Dichotomous Behavior of Capillary Surfaces in Zero Gravity," *Microgravity Science and Technology*, Vol. 3, No. 2, 1990, pp. 87–92.

[11]Smedley, G., "Containments for Liquids at Zero Gravity," *Microgravity Science and Technology*, Vol. 3, 1990, pp. 13–23.

[12]Langbein, D., Grossbach, R., and Heide, W., "Parabolic Flight Experiments on Fluid Surfaces and Wetting," *Applied Microgravity Technology*, Vol. 2, No. 4, 1990, pp. 198–211.

[13]Smedley, G., "Preliminary Drop-Tower Experiments on Liquid-Interface Geometry in Partially Filled Container at Zero Gravity," *Experiments in Fluids*, Vol. 8, 1990, pp. 312–318.

[14]Collicott, S. H., and Weislogel, M. M., "Corner Radius Effects on Capillary Instability in Tank Geometries," AIAA Paper 2001-3824, July 2001.

[15]Concus, P., and Finn, R., "On the Behavior of a Capillary Surface in a Wedge," *Applied Mathematical Sciences*, Vol. 63, No. 2, 1969, pp. 292–299.

[16]Concus, P., and Finn, R., "Capillary Surfaces in a Wedge—Differing Contact Angles," *Microgravity Science and Technology*, Vol. 7, No. 2, 1994, pp. 152–155.

[17]Concus, P., and Finn, R., "Capillary Wedges Revisited," *SIAM Journal on Mathematical Analysis*, Vol. 27, No 1, 1996, pp. 56–69.

[18]Dreyer, M., Delgado, A., and Rath, H.-J., "Fluid Motion in Capillary Vanes Under Reduced Gravity," *Microgravity Science and Technology*, Vol. 5, No. 4, 1993, pp. 203–210.

[19]Brakke, K. A., "The Surface Evolver," *Experimental Mathematics*, Vol. 1, 1992, pp. 141–165.

[20]Chandra, B. W., and Collicott, S. H., "Low-Gravity Propellant Slosh Using Surface Evolver," AIAA Paper 2002-3981, July 2002.

[21]Tegart, J., "Three-Dimensional Fluid Interfaces in Cylindrical Containers," AIAA Paper 91-2174, June 1991.

[22]Brakke, K. A., "Stability of Torus Bubble in Rotating Tank," Lockheed Research Lab., CR, Palo Alto, CA, 1993.

[23]Collicott, S. H., Bayt, R. L., and Courtney, S. D., "Ullage Bubble Stability in the Gravity Probe-B Helium Tank," AIAA Paper 94-3026, June 1994.

[24]Bayt, R. L., and Collicott, S. H., "Effects of an Elliptic End-Cap on the Ullage Bubble Stability in the Gravity Probe-B Satellite," AIAA Paper 96-0596, Jan. 1996.

[25]Chen, Y., and Collicott, S. H., "Effects of Wicking and Spin on Bubble Position in the Gravity Probe-B Helium Tank Geometry," AIAA Paper 2002-1004, Jan. 2002.

[26]Concus, P., Finn, R., and Weislogel, M. M., "Capillary Surfaces in an Exotic Container: Results from Space Experiments," *Journal of Fluid Mechanics*, Vol. 394, 1999, pp. 119–135.

[27]Collicott, S. H., "Asymmetric Propellant Positions in Symmetric Tanks and Vanes," AIAA Paper 2003-4892, July 2003.

[28]Concus, P., Finn, R., and Zabihi, F., "On Canonical Cylinder Sections for Accurate Determination of Contact Angle in Microgravity," *Fluid Mechanics Phenomena in Microgravity*, AMD-Vol. 154/FED-Vol. 142, American Society of Mechanical Engineers, Fairfield, NJ, 1992, pp. 125–131.

[29]Chen, Y., and Collicott, S. H., "A New Design of Drop Tower to Study Uncertainties in Zero-Gravity Fluid Mechanics," AIAA Paper 2001-0609, Jan. 2001.

[30]Weislogel, M. M., "Capillary Flow in Interior Corners: The Infinite Column," *Physics of Fluids*, Vol. 13, No. 11, 2001, pp. 3101–3107.

[31]Washburn, E., "The Dynamics of Capillary Flow," *Physical Review*, Vol. 17, No. 3, 1921, pp. 273–283.

[32]Dreyer, M., Delgado, A., and Rath, H.-J., "Capillary Rise of Liquid Between Parallel Plates Under Microgravity," *Journal of Colloid and Interfacial Science*, Vol. 163, 1994, pp. 158–168.

[33]Clanet, C., and Quere, D., "Onset of Menisci," *Journal of Fluid Mechanics*, Vol. 460, 2002, pp. 131–149.

S. Mahalingam
Associate Editor